3D-Pharmacophere Models for CC Chemokine Receptor 1 Antagonists

Yixi Liu, Philippe Andre, Jing Wei* and Kang Zhao*

Tianjin Key Laboratory for Modern Drug Delivery & High-Efficiency, School of Pharmaceutical Science and Technology, Tianjin University, 92 Weijin Road, Nankai District, Tianjin 300072, China

Abstract: The CC Chemokine Receptor 1 (CCR1) is closely related to various chronic inflammatory diseases like rheumatoid arthritis and multiple sclerosis, and plays a crucial role in transplant rejection. Inhibiting its activity with CCR1 antagonists has been proved to be effective in preventing some diseases. A number of *in vivo* experiments have been carried out to shed light on the underlying mechanism of the interactions between the CCR1 and its ligands. However, their conclusions are still controversial. In this study, ligand-based computational drug design is applied as a new and effective way to study the structure-activity relationship of CCR1 antagonists. Three-dimensional pharmacophore models were generated for CCR1 antagonists, using both HypoGen and HipHop algorithms in Catalyst software. Two optimal pharmacophore models were defined through careful qualification processes. Both of them have four features: one hydrogen-bond acceptor, one positive ionable and two hydrophobic groups. Additional information was obtained through comparison between the two models. Our results can be valuable tools for the discovery and development of specific, highly potent CCR1 antagonists. For Supplement material, please see the online version of the article.

For Supplement material, please see the online version of the article.

Key Words: Chemokine, CC chemokine receptor 1 antagonist, pharmacophore model.

INTRODUCTION

Chemokines are chemotactic cytokines, a group of small proteins that play an important role in the immune response by regulating leukocyte-trafficking [1, 2]. Chemokines are mainly divided into CC and C-X-C families, based on the position of the first two cysteine residues [3]. All chemokines exert their effects by activating corresponding cell surface receptors (chemokine receptors), eliciting mobilization of immune cells against pathogenic organisms by direct recruitment and activation [4-6]. The CC Chemokine Receptor 1 (CCR1) is crucial in transplant rejection and chronic inflammatory diseases like rheumatoid arthritis and multiple sclerosis [7-12]. For these reasons, selective antagonists of CCR1 may be interesting therapeutic tools against chronic inflammatory diseases.

Several chemotypes have been described for CCR1 antagonists: xanthene-9-carboxamides, piperazines, 4-hydroxypiperidines and aminoquinolines [13-18]. Most CCR1 antagonists reported so far suffered from poor species cross-reactivity or insufficient oral bioavailability, and did not undergo further pharmacological evaluation [19]. Our objective was to generate 3D-pharmacophore models to deepen the understanding of interactions between the receptor and its ligands, and to design novel antagonists.

MATERIALS AND METHODS

In this paper, both quantitative and qualitative approaches (HypoGen and HipHop) within Catalyst 4.11 software were applied to automated pharmacophore model generation for CCR1 antagonists [20].

HypoGen Model

HypoGen aims to construct a pharmacophore that best correlates the three-dimensional arrangements of features in training compounds with the activities of those compounds. Relatively accurate experimental data are required. Thus, 26 CCR1 antagonists with xanthene-9-carboxamide structures were selected to form the HypoGen training set (Table **1**). The activities of those molecules spanned 5 orders of magnitude, from 0.9 nM to 10000 nM. Another 15 xanthene derivatives and 15 piperazine derivatives made up the test set (Tables **2**, **3**) for HypoGen model validation.

HipHop Model

The HipHop study further investigates the structure-activity relationship, calculating hypotheses by aligning those features that are common to all molecules in a given training set. Hypothesis generation is based on the conformational models of a set of compounds selected for their high activity and structural diversity; exact activity values are not needed. In our study, antagonists with three kinds of core structure (xanhene-9-carboxamide, piperazine and 4-hydroxypiperidine) were selected for the HipHop training set (eight: **23**, **25**, **39**, **40** and **57**~**60**) and test set (eleven: **13**~**15**, **20**~**22**, **24**, **26** and **61**~**63**). Their structures are showed in Fig. (**1**).

All structures were built using a 2D/3D editor-sketcher and were minimized to a local energy minimum using the CHARMm-like force field. The conformer generation for all compounds was set at a maximum of 250 conformers with an energy threshold of 15kcal/mol by means of the Poling algorithm [21]. Based on the characteristic features of the

*Address correspondence to these authors at the Tianjin Key Laboratory for Modern Drug Delivery & High-Efficiency, School of Pharmaceutical Science and Technology, Tianjin University, 92 Weijin Road, Nankai District, Tianjin 300072, China; Tel: +86-022-27404031; Fax: +86-022-27892025; E-mail: betty_wj@yahoo.com.cn; kangzhao@tju.edu.cn

1573-4064/09 $55.00+.00

Table 1. Structures of Compounds 1-26 [13]

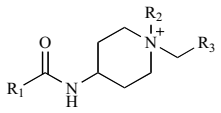

Compds	R_1	R_2	R_3
1	9-xanthenyl	H	cyclooctyl
2	9-xanthenyl	H	phenyl
3	9-xanthenyl	H	2-naphthyl
4	9-anthracenyl	H	cyclooctyl
5	diphenylmethyl	H	cyclooctyl
6	2,7-dichloro-9-xanthenyl	H	cyclooctyl
7	2,7-dibromo-9-xanthenyl	H	cyclooctyl
8	9-xanthenyl	H	1-cyclooctenyl
9	2,7-dichloro-9-xanthenyl	H	1-cyclooctenyl
10	2,7-dibromo-9-xanthenyl	H	1-cyclooctenyl
11	9-xanthenyl	methyl	cyclooctyl
12	9-xanthenyl	ethyl	cyclooctyl
13	9-xanthenyl	n-propyl	cyclooctyl
14	9-xanthenyl	n-butyl	cyclooctyl
15	9-xanthenyl	allyl	cyclooctyl
16	9-xanthenyl	phenyl	cyclooctyl
17	9-anthracenyl	methyl	cyclooctyl
18	diphenylmethyl	methyl	cyclooctyl
19	2,7-dichloro-9-xanthenyl	methyl	cyclooctyl
20	2,7-dibromo-9-xanthenyl	methyl	cyclooctyl
21	2,7-dibromo-9-xanthenyl	ethyl	cyclooctyl
22	9-xanthenyl	methyl	1- cyclooctenyl
23	9-xanthenyl	ethyl	1- cyclooctenyl
24	9-xanthenyl	n-propyl	1- cyclooctenyl
25	2,7-dichloro-9-xanthenyl	ethyl	1- cyclooctenyl
26	2,7-dibromo-9-xanthenyl	ethyl	1- cyclooctenyl

HypoGen and HipHop training-set molecules analyzed with Catalyst, the hydrogen-bond acceptor (HBA), positive ionizable (PI) and hydrophobic (H) features were selected from the feature dictionary for pharmacophore model generation.

RESULTS

HypoGen Model

Hypothesis generation based on the HypoGen training set returned ten pharmacophore models. According to the results, the first hypothesis was the best pharmacophore model characterized by the highest cost difference (71.37) and the best correlation coefficient (0.90). This was further confirmed by the validation process. We renamed this best model as Hypo-1. It consists of one HBA, one PI and two H features. The 2D representation of the Hypo-1 model and distances between its features is shown in Fig. (**2**).

Table 2. Structures of Compounds 27-41 [14]

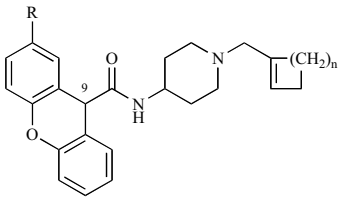

No.	R	n
27	H	3
28	H	4
29	H	5
30	H	6
31	$NHCO_2Allyl$	6
32	$CONHCH_2C_6H_4$(2-OMe)	6
33	$CONHCH_2C_6H_4$(4-OMe)	6
34	$CONHCH_2$(4-pyridylmethyl)	6
35	OCNH(4-piperidine)	6
36	OCNH(4-piperidine)	5
37	$OCNH(CH_2)_3NH_2$	6
38	OC(4'-NH_2)piperidine	6
39	OC(3'-CH_2NH_2)piperidine	6
40	OC(3'R-CH_2NH_2)piperidine	6
41	9S-OC(3'S-CH_2NH_2)piperidine	6

Table **4** shows the actual and estimated Ki inhibitory activities of the HypoGen training set based on Hypo-1. All compounds in this study were classified according to their activity as 'highly active' (≤10 nM, +++), 'moderately active' (10 nM～1000 nM, ++), or 'inactive' (≥1000 nM, +). All inactive compounds were correctly predicted, two moderately active compounds were predicted to be highly active and one was predicted as inactive. All but four of the highly active compounds were predicted correctly. Altogether, for 19 out of 26 compounds, the predicted Ki values were found to be within the same scale as the experimentally determined ones. Finally, in order to further assess the predictive power of Hypo-1, the activities of the 30 test-set compounds were evaluated. About 87% of them had experimental and estimated activities falling within the same range (supplement Table **S1**). Hypo-1 was regressed using each molecule in the training and test sets. The regression line shown in Fig. (**3**) indicates a good correlation between measured and estimated activities. All the facts above strongly confirmed the reliable ability of our model to predict the activity of compounds.

Table 3. Structures of Compounds 42-56 [15]

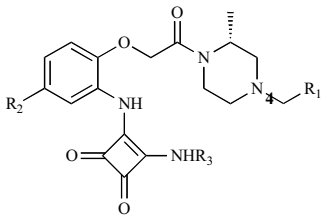

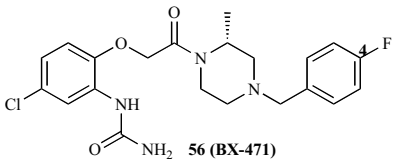

56 (BX-471)

No.	R_1	R_2	R_3
42	Ph	Cl	Me
43	4-chlorophenyl	Cl	Me
44	2-fluorophenyl	Cl	Me
45	3-fluorophenyl	Cl	Me
46	5-chloro-2-thienyl	Cl	Me
47	4-chlorophenyl (des-methyl piperazine)	Cl	Me
48	4-fluorophenyl	H	Me
49	4-fluorophenyl	Me	Me
50	4-fluorophenyl	Cl	Et
51	4-fluorophenyl	Cl	CH_2Ph
52	4-fluorophenyl	Cl	$(CH_2)_2N(CH_3)_2$
53	4-fluorophenyl	Cl	$(CH_2)_2OH$
54	4-fluorophenyl	Cl	$(CH_2)_2$pyrrole
55	4-fluorophenyl	Cl	CH_2(2-pyridyl)

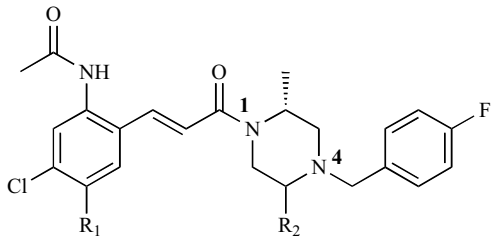

57[16] R_1=OMe R_2=H

58[16] R_1=H R_2=(S)-Me

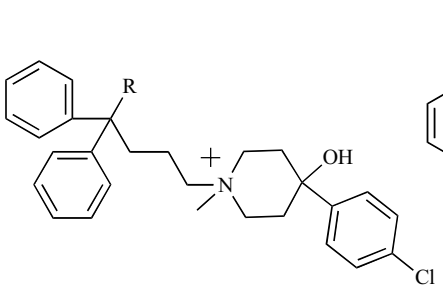

59[17] R=H

60[17] R=CN

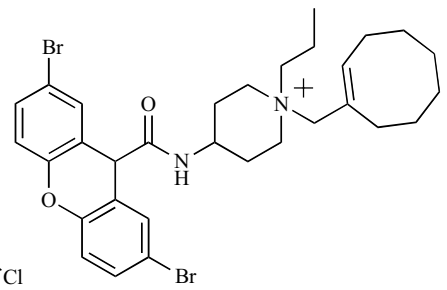

61[13]

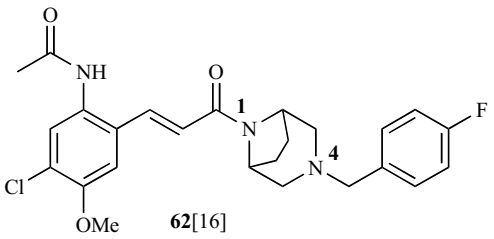

62[16]

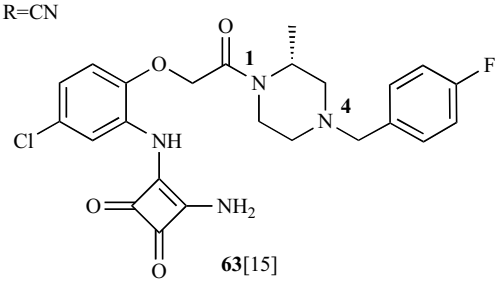

63[15]

Fig. (1). Structures of some HipHop compounds.

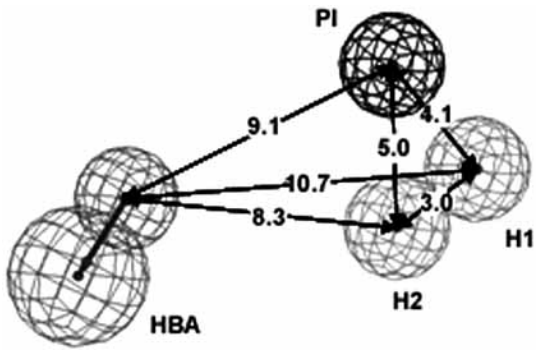

Fig. (2). Hypo-1, the best quantitative model.

The affinities of highly active xanthene-9-carboxamide derivatives were correctly estimated, thanks to the possibility of complete mapping of those molecules onto the model. In their case, the HBA feature was occupied by the oxygen on the xanthene ring, the PI region mapped to the piperidine nitrogen (or quaternary ammonium nitrogen), whereas the cyclooctyl (or 1-cyclooctenyl) moiety mapped to the two H features. See **25** in Fig. (**4A**).

Table 4. Experimental Biological Data and Estimated Ki of Compounds in the HypoGen Training Set Based on Hypo-1

No.	Act Ki [nM]	Est Ki [nM]	Act Scale[a]	Est Scale[a]
25	0.9	3.5	+++	+++
26	1.9	4.3	+++	+++
23	2.0	3.0	+++	+++
22	2.5	6.4	+++	+++
24	2.8	8.8	+++	+++
21	3.3	27	+++	++
13	3.6	51	+++	++
20	3.9	4.4	+++	+++
14	5.0	3.4	+++	+++
12	5.2	18	+++	++
15	9.7	12	+++	++
11	14	5.4	++	+++
19	17	4.7	++	+++
8	51	390	++	++
1	140	16	++	++
10	150	62	++	++

(Table 4. Contd….)

9	200	950	++	++
16	370	81	++	++
18	800	1300	++	+
5	1100	1200	+	+
17	1800	1200	+	+
7	5100	1200	+	+
4	10000	1200	+	+
3	10000	3200	+	+
2	10000	1500	+	+
6	10000	1300	+	+

[a]Activity scale: highly active (≤10 nM, +++), moderately active (10 nM<Activity≤1000 nM, ++), and inactive (>1000 nM, +).

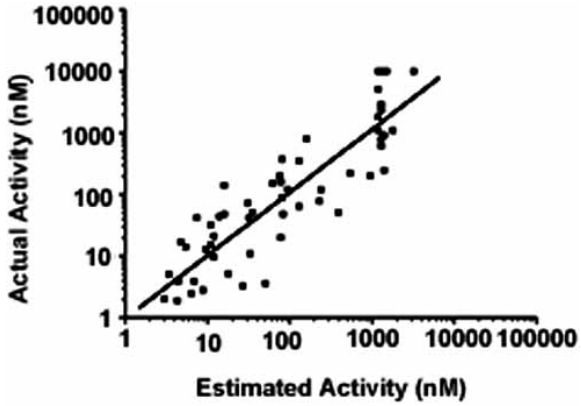

Fig. (3). Plot of predicted activities against experimental values (Ki in nM).

Our analyses highlighted some differences in the fitting mode of the piperazine derivatives. Their mapping results indicated that the 4-piperazine nitrogen mapped to the PI feature. The chlorophenyl (or fluorophenyl) on the piperazine cycle, together with the chlorine atom (or methyl) on the middle phenyl ring form a large hydrophobic group that could occupy both H1 and H2, just like the cyclooctyl (or 1-cyclooctenyl) moiety in xanthene derivatives. The HBA region was occupied by the diaminocyclobutenedione group. See **53** in Fig. (**4B**).

The mapping analysis suggested that the inability of some inactive compounds, such as **4, 5, 17** and **18,** to map with the HBA feature of Hypo-1 was due to their lack of xanthene oxygen atom (supplement Fig. (**S1**)). This fact accounted for an approximately 10-fold reduction in activity when the xanthen-9-yl moiety of **1** was replaced with an anthracen-9-yl (**4**) or diphenylmethyl (**5**) [13]. Another interesting molecule was **56** (**BX-471**). Its urea group, compared to the diaminocyclobutenedione moiety in other piperazine derivatives, was too small to reach the HBA region concur-

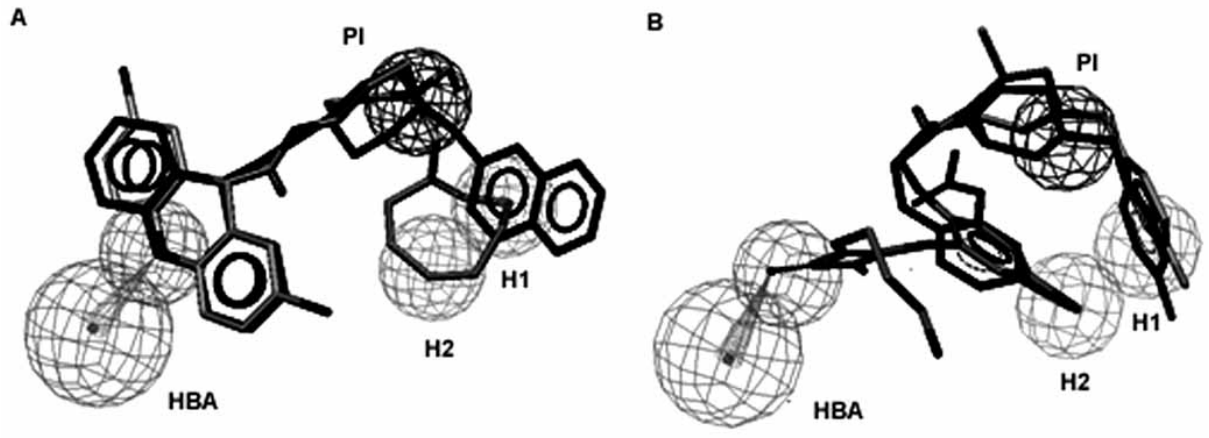

Fig. (4). The Hypo-1 model mapped with some of the HypoGen compounds (A. **3** and **25**; B. **53** and **56**).

rently with the mapping of the terminal fluorophenyl group to the H2 feature. However**,** replacement of the urea moiety with a diaminocyclobutenedione (**54** and **55**) enhanced the antagonist activity, as it makes the molecules recover the HBA feature (Fig. **4B**). All the facts above indicated that the HBA feature in Hypo-1 is essential for high activity. Therefore, both the xanthene group in xanthen-9-carboxamide derivatives and the diaminocyclobutenedione moiety in piperazine derivatives work as hydrogen-bond acceptors to improve the binding affinity.

Additionally, we found that compounds mapping poorly to the H1 and H2 features in Hypo-1 were inactive. This fact confirmed that the presence of the two H features is critical for high activity. In most of the training-set compounds, the terminal groups on the piperazine cycle were big hydrophobic rings, such as cyclooctane (or cyclooctene), which could fully occupy the two H features. However, the small phenyl ring in **2** could map only one H feature. Although **3** possessed a large 2-naphthylmethyl, it could not simultaneously map the two H features because of its rigid conformation. Both those compounds adopted a conformation that mapped H1 in the upper place but not H2 in the downer place (**3** in Fig. (**4A**) and supplement Fig. (**S2A**)). Also, while the PI and HBA features could be mapped by most ligands in the test set, the two H features can be mapped only if the volume of the ligands' terminal hydrophobic groups is big enough. For example, **27** and **28**, which have terminal hydrophobic rings composed of six or seven atoms, were inactive due to the difficulty in mapping with the two features simultaneously (supplement Fig. (**S2B**). This was in good agreement with experimental data. As discussed by Naya's group in their SAR study, the voluminal minification of the terminal chemical group results in a loss in antagonist activity [14]. Corresponding to the two H features, there is probably a hydrophobic pocket with a radius of more than 3.0 Å on the receptor site (Fig. (**2**)).

In addition, compared to the para-substituted terminal benzyl in most piperazine derivatives, the ortho or meta substitutions in **44** and **45** lowered the activity. Fig. (**5**) shows the overlay of **44** and **45** mappings onto Hypo-1. When the terminal benzyl fully occupies the H1 feature, the fluorine at the ortho- or meta-position causes some sort of stereospecific blockade that prevents the mapping of the middle benzyl with H2. **44** entirely missed H2, while the meta-fluorine of **45** could map only partly to H2. Therefore, neither molecule adopted a conformation that could fully map both H features simultaneously. In fact, experimental data showed that those substitution transpositions significantly reduced potency (by over 2000 nM).

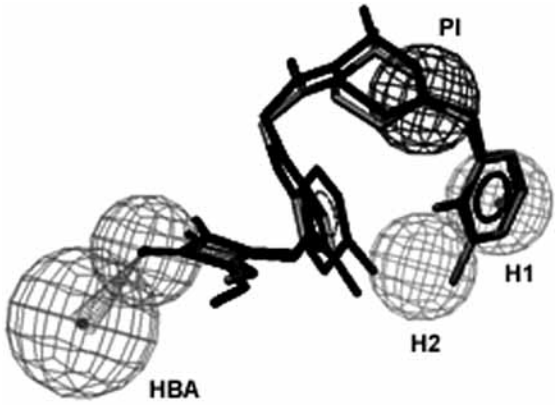

Fig. (5). The Hypo-1 mapped with **44** and **45**.

HipHop Model

Furthermore, ten hypotheses were selected on the basis of high ranking scores in the HipHop module. The statistically best model obtained through validation of the training and test sets was renamed as Hypo-2. It contained one HBA, one PI and two H features. To distinguish these features from those of Hypo-1, they are marked in italics (*HBA*, *PI*, *H1* and *H2*). The 2D hypotheses and distances between the features of Hypo-2 are shown in Fig. (**6**).

Our best-fit analysis of the mapping of all 19 compounds (from HipHop training and test sets) to Hypo-2 revealed that they possess all four features of Hypo-2. Their average predicted best-fit value was 3.9 (supplement Table **S2**). Mapping results showed that compounds with various structures map with all features of Hypo-2, and that Hypo-2 is able to successfully identify all the crucial features common to highly potent CCR1 antagonists.

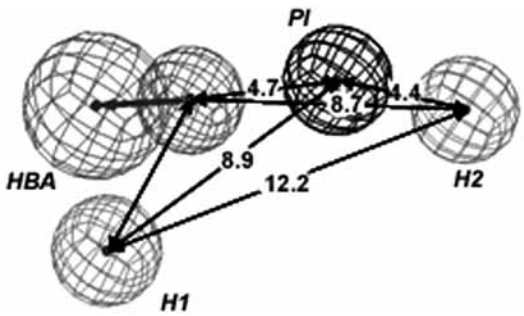

Fig. (6). Hypo-2, the best qualitative model.

Fig. (**7**) shows the mappings of different structural compounds onto Hypo-2. For xanthene-9-carboxamide derivatives, the *H1* feature mapped the chlorine atom at position 2 or 7 of the xanthene group, the *HBA* feature was occupied by the carbonyl oxygen, the piperidine nitrogen mapped to the *PI* region like in Hypo-1, and the *H2* feature was occupied by the terminal hydrophobic functional group (cyclooctane or cyclooctene). The mappings of this class onto Hypo-2 are shown in supplement Fig. (**S3**).

57 and **58** were overlaid and mapped onto Hypo-2, as shown in Fig. (**7A**). The *PI* region was occupied by the 4-piperazine nitrogen atom, and the *H2* feature mapped the 4-fluorophenyl on the piperazine cycle. As for the substitution on the 1-piperazine nitrogen, the *HBA* feature was occupied by the carbonyl oxygen on the bicycle[2.2.2]octane ring, and the *H1* feature was occupied by the terminal phenyl ring. Furthermore, **62** and **63**, as analogues of **57**, showed a similar mapping with Hypo-2.

For **59** and **60** (Fig. **7B**), the *PI* region interacted with their quaternarized piperidine nitrogen atom, and the *H2* feature mapped either one of the phenyl rings. For the 4-hydroxy-4-phenylpiperidine group, the *HBA* feature was occupied by the hydroxyl group, while the *H1* feature mapped the chlorine atom on the phenyl ring.

Through validation of the models and mapping analyses, we identified four features in Hypo-1 that seemed to be necessary for high antagonist activity. Hypo-2 contained the same number of seemingly essential features. A superimposition (Fig. (**8**)) of the two models showed that the PI and H1 features almost exactly matched PI and H2, respectively. The other features had no match in the other model. We thus theorized that the receptor site has a big pocket that includes PI/*PI* and H1/*H2* and the four other features (HBA, H2, *H1* and *HBA*), but that PI/*PI* and H1/*H2* are the most essential for ligand-receptor binding. Antagonist activity requires functional groups that can map with the PI/*PI* and H1/*H2* features, but higher affinity is achieved when other functional groups map with the other four features to some extend, no matter whether those features belong to Hypo-1 or Hypo-2. The more complete the mapping, the higher the affinity would be. We found that compounds **3** and **25** in Fig. (**4A**) can illustrate that idea. They both could map to the HBA, PI and H1 features, but differed in that **25** could additionally map to H2. This difference would explain the fact that the antagonist activity of **25** is 10000 times higher than that of **3**.

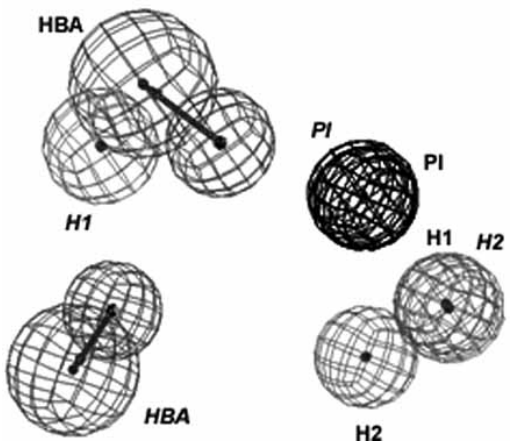

Fig. (8). Comparison of Hypo-1 and Hypo-2.

CONCLUSION

A ligand-based computational approach was used to study the molecular structure-activity relationship of CCR1 antagonists. A highly predictive pharmacophore model (Hypo-1) was generated, consisting of one HBA, one PI, and

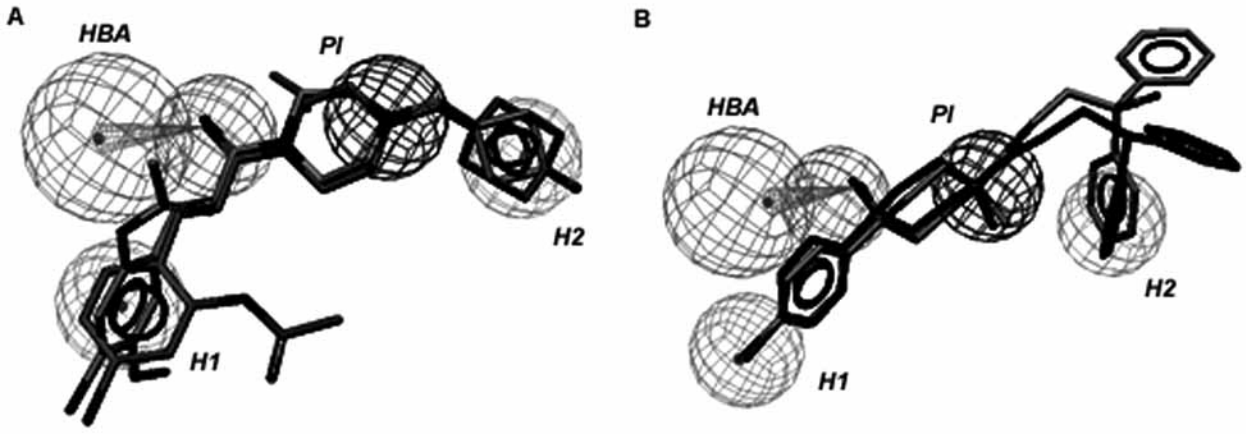

Fig. (7). The Hypo-2 model mapped with some of the HipHop compounds (A **57** and **58**; B **59** and **60**).

two H features. The mapping analysis of the two H features established that the receptor site includes a hydrophobic pocket with a radius of more than 3.0 Å. Thus, a hydrophobic group of proper size is essential for high docking affinity. Hypo-2, our qualitative pharmacophore model possesses features that are similar, in type and number, to those of Hypo-1. However, a closer comparison between the two models showed that only the PI and H1 features in Hypo-1 and *PI* and *H2* features in Hypo-2 are located at matching sites on the receptor. Therefore, the design of novel CCR1 antagonists should primarily focus on those PI/*PI* and H1/*H2* features. We also highlighted the importance of other features like HBA and H2 for higher antagonist activity. Hence, our models can serve as a three-dimensional query in database screening to facilitate the discovery and development of new lead-compounds with high CCR1 antagonist activity.

ACKNOWLEDGEMENTS

With special thanks to Mr. Yingda Ye for his dedicated support to this study.

REFERENCES

[1] Baggiolini, M. Chemokines and leukocyte traffic. *Nature*, **1998**, *392*, 565-8.

[2] Strieter, R.M.; Standiford, T.J.; Huffnagle, G.B.; Colletti, L.M.; Lukacs, N.W.; Kunkel, S.L. "The good, the bad, and the ugly": the role of chemokines in models of human disease–commentary. *J. Immunol.*, **1996**, *156*, 3583-6.

[3] Murphy, P.M.; Baggiolini, M.; Charo, I.F.; Hebert, C.A.; Horuk, R.; Matsushima, K.; Miller, L.H.; Oppenheim, J.J.; Power, C.A. Power, international union of pharmacology. XXII. Nomenclature for chemokine receptors. *Phamacol. Rev.*, **2000**, *52*, 145-76.

[4] Dohlman, H.G.; Thorner, J.; Caron, M.G.; Lefkowitz, R.J. Model systems for the study of seven transmembrane segment receptors. *Ann. Rev. Biochem.*, **1991**, *60*, 653-88.

[5] Horn, F.; Weare, J.; Beukers, M.W.; Horsch, S.; Bairoch, A.; Chen, W.; Edvardsen, O.; Campagne, F.; Vriend, G. GPCRDB: an information system for G protein-coupled receptors. *Nucleic Acids Res.*, **1998**, *26,* 275-9.

[6] Luster, A.D. Mechanisms of disease: chemokines– chemotactic cytokines that mediate inflammation. *N. Engl. J. Med.*, **1998**, *338*, 436-45.

[7] Pattison, J.M.; Nelson, P.J.; Huie, P.; Von, L.I.; Farshid, G.; Sibley, R.K.; Krensky, A.M. RANTES chemokine expression in cell-mediated transplant rejection of the kidney. *Lancet*, **1994**, *343*, 209-11.

[8] Pattison, J.M.; Nelson, P.J.; Huie, P.; Sibley, R.K.; Krensky, A.M. RANTES chemokine expression in transplantassociated accelerated atherosclerosis. *J. Hearth. Lung Transpl.*, **1996**, *15,* 1194-9.

[9] Koch, A.E.; Kunkel, S.L.; Strieter, R.M. Cytokine in rheumatoid arthritis. *J. Invest. Med.*, **1995**, *43*, 28-38.

[10] Snowden, N.; Hajeer, A.; Thomson, W.; Ollier, B. RANTES role in rheumatoid arthritis. *Lancet*, **1994**, *343*, 547-8.

[11] Hvas, J.; Mclean, C.; Justesen, J.; Kannourakis, G.; Steinman, L.; Oksenberg, J.R.; Bernard, C.C.A. Perivascular T cells express the pro-inflammatory chemokine RANTES mRNA in multiple sclerosis lesions. *Scand. J. Immunol.*, **1997**, *46*, 195-203.

[12] Glabinski, A.R.; Tani, M.; Tuohy, V.K.; Ransohoff, R.M. Murine experimental autoimmune encephalomyelitis: A model of immune-mediated inflammation and multiple sclerosis. *Methods Enzymol.*, **1997**, *288*, 182-9.

[13] Naya, A.; Sagara, Y.; Ohwaki, K.; Saeki, T.; Ichikawa, D.; Iwasawa, Y.; Noguchi, K.; Ohtake, N. Design, synthesis, and discovery of a novel CCR1 antagonist. *J. Med. Chem.*, **2001**, *44*, 1429-35.

[14] Naya, A.; Ishikawa, M.; Matsuda, K.; Ohwaki, K.; Saeki, T.; Noguchi, K.; Ohtake, N. Structure–activity relationships of xanthene carboxamides, novel CCR1 receptor antagonists. *Bioorg. Med. Chem.*, **2003**, *11*, 875-84.

[15] Xie, Y.F.; Lake, K.; Ligsay, K.; Komandla, M.; Sircar, I.; Nagarajan, G.; Li, J.; Xu, K.; Parise, J.; Schneider, L.; Huang, D.; Liu, J.P.; Dines, K.; Sakurai, N.; Barbosab, M.; Jack, R. Structure–activity relationships of novel, highly potent, selective, and orally active CCR1 antagonists. *Bioorg. Med. Chem. Lett,*, **2007**, *17*, 3367-72.

[16] Revesz, L.; Bollbuck, B.; Buhl, T.; Eder, J.; Esser, R.; Feifel, R.; Heng, R.; Hiestand, P.; Demange, B.J.; Loetscher, P.; Sparrer, H.; Schlapbach, A.; Waelchli, R. Novel CCR1 antagonists with oral activity in the mouse collagen induced arthritis. *Bioorg. Med. Chem. Lett.*, **2005**, *15*, 5160-4.

[17] Ng, H.P.; May, K.; Bauman, J.G.; Ghannam, A.; Islam, I.; Liang, M.N. Horuk, R.; Hesselgesser, J.; Snider, R.M.; Perez, H.D.; Morrissey, M.M. Discovery of novel non-peptide CCR1 receptor antagonists. *J. Med. Chem.*, **1999**, *42*, 4680-94.

[18] Brown, M.F.; Avery, M.; Brissette, W.H.; Chang, J.H.; Colizza, K.; Conklyn, M.; DiRico, A.P.; Gladue, R.P.; Kath, J.C.; Krueger, S.S.; Lira, P.D.; Lillie, B.M.; Lundquist, G.D.; Mairs, E.N.; McElroy, E.B.; McGlynn, M.A.; Paradis, T.J.; Poss, C.S.; Rossulek, M.I.; Shepard, R.M.; Sims, J.; Strelevitz, T.J.; Truesdell, S.; Tylaska, L.A.; Yoon, K.; Zheng D.Y. Novel CCR1 antagonists with improved metabolic stability. *Bioorg. Med. Chem. Lett.*, **2004**, *14*, 2175-9.

[19] Horuk, R.; Ng, H.P. Chemokine receptor antagonists. *Med. Res. Rev.*, **2000**, *202*, 155-68.

[20] CATALYST 4.11, User Guide, Accelrys, San Diego, CA, USA, **2006**.

[21] Smellie, A.; Teig, S.L.; Towbin, P. Poling: promoting conformational variation. *J. Comput. Chem.*, **1995**, *16*, 171-87.

Received: 15 January, 2009 **Revised: 07 March, 2009** **Accepted: 15 March, 2009**